Digital Twin Enabled Domain Adversarial Graph Networks for Bearing Fault Diagnosis

Ke Feng, *Member, IEEE*, Yadong Xu, Yulin Wang, Sheng Li, Qiubo Jiang, Beibei Sun, Jinde Zheng, and Qing Ni

***Abstract*—The fault diagnosis of rolling bearings is of utmost importance in industrial applications to ensure mechanical systems' reliability, safety, and economic viability. However, conventional data-driven fault diagnosis techniques mainly depend on a pre-existing dataset with complete failure modes and knowledge to serve as the training data, which may not be available or accessible in some crucial industrial scenarios. This can limit the practicality of these methodologies in real-world industrial applications. This article addresses this issue by developing a novel digital twin-enabled domain adversarial graph network (DT-DAGN). The main contributions of this article are as follows: 1) the development of a comprehensive and accurate digital twin model for rolling bearings that includes a dynamic simulation of the bearing's operational status using only its structural parameters and failure severity/size to obtain the system's vibration response, and 2) the development of a novel graph convolutional network-based transfer learning framework to transfer knowledge from simulated datasets to measured datasets, enabling effective fault diagnostics of bearings with limited knowledge. A series of experiments are applied to validate the efficacy of the developed methodology.**

***Index Terms*—Digital twin, digital twin enabled domain adversarial graph network (DT-DAGN), fault diagnosis, limited knowledge, rolling bearing.**

Manuscript received 8 May 2023; revised 29 June 2023; accepted 18 July 2023. Date of publication 26 July 2023; date of current version 3 August 2023. This work was supported in part by the National Key Research and Development Program of China under Grant 2022YFB3402100 and in part by the National Natural Science Foundation of China under Grant 51975004. *(Corresponding authors: Yadong Xu; Yulin Wang; Jinde Zheng.)*

Ke Feng is with the Department of Industrial Systems Engineering and Management, National University of Singapore, Singapore 119077 (e-mail: ke.feng@nus.edu.sg; ke.feng@outlook.com.au).

Yadong Xu and Yulin Wang are with the School of Mechanical Engineering, Nanjing University of Science and Technology, Nanjing 210094, China (e-mail: ydxu@seu.edu.cn; wyl_sjtu@126.com).

Sheng Li is with the Bussiness School, Hohai University, Nanjing 211100, China (e-mail: shengli@hhu.edu.com).

Qiubo Jiang and Beibei Sun are with the School of Mechanical Engineering, Southeast University, Nanjing 211189, China (e-mail: jiangqb@seu.edu.cn; bbsun@seu.edu.cn).

Jinde Zheng is with the School of Mechanical Engineering, Anhui University of Technology, Maanshan 243099, China (e-mail: jdzheng@ahut.edu.cn).

Qing Ni is with the School of Mechanical and Mechatronic Engineering, University of Technology Sydney, Sydney, NSW 2007, Australia (e-mail: qing.ni@outlook.com.au).

Digital Object Identifier 10.1109/TICPS.2023.3298879

I. Introduction

As INDUSTRIAL equipment becomes increasingly advanced and automated, implementing real-time and effective condition monitoring and health management has become urgent. Rolling bearing malfunctions and failures can have detrimental effects on the reliable operations of equipment, and in severe cases, may even result in catastrophic accidents. Therefore, it is crucial to prioritize the development of strategies or methodologies to monitor and diagnose equipment operating conditions and health status in a real-time manner [1].

Conventional diagnostic methodologies mainly utilise signal analysis techniques that rely on expert knowledge to extract fault characteristics and features. For example, Yan et al. [2] proposed a multiscale dispersion entropy to measure the complexity of mechanical signals and used it for machinery fault detection. Xu et al. [3] introduced an adaptive signal reconstruction method to pinpoint fault-related information in vibration signals. Chen et al. [4] proposed a sparse multivariate model-based approach to assess the damage degree of rotating machinery. Nevertheless, these methodologies are often time-consuming and labour-intensive, with limitations in effectively identifying non-smooth and non-linear attributes of mechanical signals, particularly in challenging operational environments [5]. Conventional diagnostic methodologies mainly utilize signal analysis techniques that rely on expert knowledge to extract fault characteristics and features. For example,Yan et al. [2] proposed a multiscale dispersion entropy to measure the complexity of mechanical signals and used it for machinery fault detection. Xu et al. [3] introduced an adaptive signal reconstruction method to pinpoint fault-related information in vibration signals. Chen et al. [4] proposed a sparse multivariate model-based approach to assess the damage degree of rotating machinery. Nevertheless, these methodologies are often time-consuming and labor-intensive, with limitations in effectively identifying non-smooth and non-linear attributes of mechanical signals, particularly in challenging operational environments [5], [6].

In recent times, the field of deep learning has made significant advancements in pattern recognition, rendering it a promising and powerful tool for diagnosing machine faults. It addresses the shortcomings of conventional data-driven algorithms, thereby overcoming their limitations and opening up new possibilities for more effective fault diagnosis in bearings. By leveraging deep learning techniques, it is possible to improve the accuracy of fault diagnosis while reducing the amount of time and effort

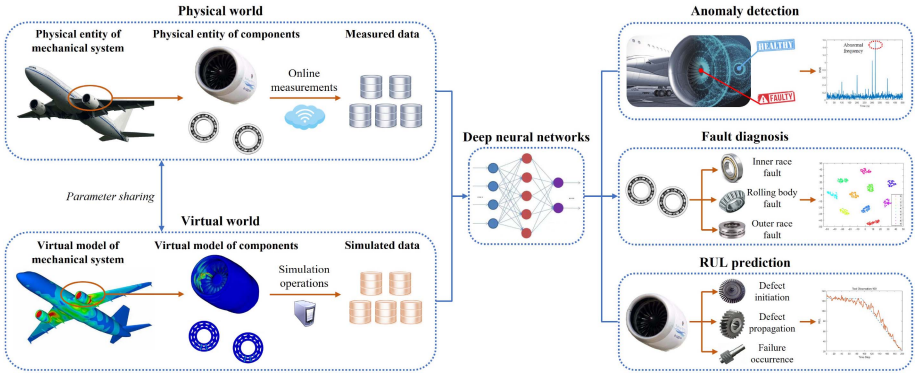

Fig. 1. Digital twin-based machinery prognostics and health management.

required for analysis. For instance, Xu et al. [7] developed a multireceptive field CNN algorithm for machine fault diagnosis under noisy conditions. Wang et al. [8] introduced a novel approach that utilizes an attention-based convolutional neural network (CNN), allowing for precise attention alignment to specific sub-tasks. Xu et al. [9] proposed a fusion CNN algorithm for effective fault recognition of machines, while the researchers of study [10] developed a CNN model with a hierarchical structure for multiscale feature extraction of mechanical signals. Han et al. [11] introduced a novel out-of-distribution detection framework that considers the uncertainty of intelligent diagnosis decisions, enhancing the trustworthiness of machinery fault diagnosis. Xu et al. [12] proposed a simple yet effective multiattention-based CNN algorithm for reliable fault diagnosis results. In research [13], a new convolutional algorithm was developed for reliable fault detection in transmission systems. These approaches have significantly contributed to the advancement of fault diagnosis techniques, driving the field forward.

In industrial practice, training and testing data often exhibit different distributions, leading to distribution discrepancies. Unsupervised domain adaptation is a promising technique for addressing this issue [14]. Zhang et al. [15] proposed a multisensor-based cross-domain CNN model for feature extraction in rotating machinery, while Zhao et al. [16] developed a federated cross-domain algorithm for machinery diagnosis. Chen et al. [17] presented a domain adversarial transfer CNN algorithm for bearing fault diagnosis, and Li et al. [18] introduced deep generative-based domain adaptation approaches for bearing condition monitoring. Shi et al. [19] developed a transferable adaptive cross-domain algorithm for machine fault diagnosis, and Yang et al. [20] developed a cross-domain diagnostic framework for fault detection under imbalanced conditions. Chen et al. [21] proposed a feature representation alignment-based CNN approach for machine health management. Li et al. [22] introduced a multi-classifier optimization-based cross-domain CNN model for machine fault diagnosis. A class-weighted adversarial CNN algorithm was developed by Li et al. [23] for cross-domain fault diagnostics of rolling bearings. Feng et al. [24] proposed a globally localized multisource domain adaptation-based approach for bearing fault diagnostics. However, the present cross-domain fault diagnosis approaches require diagnostic knowledge from source domain data, including data on condition monitoring for all possible failure modes/types. This task can be particularly challenging for certain types of bearings that seldom undergo failure. As a result, conventional domain adaptation approaches may not be effective in these situations.

The digital twin (DT) technique has emerged as a promising tool to provide reliable diagnostic knowledge for the target domain, as it enables seamless integration between the virtual and physical realms. By generating highly accurate digital representations of physical entities, DTs simulate realistic data that closely mimics the behaviour and performance of actual systems. In many industrial sectors, DT technology is being adopted as a solution to the lack of labelled data. One area where this trend is particularly evident is in the study of machinery health management. Digital twin-based tasks, as illustrated in Fig. 1, allow for comprehensive monitoring and management of machinery health throughout its entire life cycle, thanks to creating a high-fidelity virtual replica of the physical object. In the literature, several researchers have proposed digital twin-driven methodologies for machinery health management. For instance, Zhang et al. [25] proposed a digital twin-driven cross-domain diagnostic framework for machinery health management. The framework involves building a DT model to obtain reliable source domain knowledge, followed by utilizing a partial domain adaptation model for bearing fault detection. Similarly, Xiao et al. [26] developed a collaborative domain network-based diagnostic approach for bearing health assessment that bridges the gap between simulated data and real-world measured datasets. Wang et al. [27] introduced a framework of diagnostics for detecting unbalance faults of rotors using decision tree analysis. In order to improve the model's adaptability, the researchers also developed a strategy for conducting model reliability analysis and parameter sensitivity analysis. In a series of studies, Feng et al. [28], [29], [30] conducted comprehensive research on system degradation prediction using digital twin-based approaches. Their work involved the use of advanced vibration analysis techniques in combination with modelling techniques to achieve precise and reliable degradation prediction for complex systems. In a recent study, the practical digital framework presented by Feng et al. [31] employs transfer learning techniques to accurately assess gearbox transmission

degradation. This approach combines digital twin technology and transfer learning methods to provide a highly effective approach to evaluating transmission system health status. The adoption of simulation-based data-driven techniques presents a promising avenue for diminishing the need for labeled empirical data in machinery health management.

The digital twin technique holds promise for generating synthetic data to simulate imperceptible fault scenarios, enabling reliable unsupervised fault detection. However, certain significant challenges hinder the widespread adoption of digital twin techniques in machinery diagnosis. Creating a comprehensive and accurate digital twin model that reflects various severities, types, and operation conditions of rolling bearings is the primary challenge. Developing such a dynamic model for different bearings can be time-consuming and demanding, requiring significant expert knowledge. Additionally, the difference in data distribution between the simulated and measured domains presents another challenge in the context of rolling bearings. Rolling bearings often exhibit multiple fault conditions, resulting in distinct feature distribution differences across each health condition when comparing data from different domains.

To tackle the obstacles mentioned earlier, the current study presents a digital twin-based domain adversarial graph network (DT-DAGN). Firstly, a detailed and precise digital twin model is created for rolling bearings, which incorporates a dynamic simulation of the bearing's operational conditions based solely on the bearing's structural parameters and fault size/severity to generate the system vibration response. Next, a transfer learning framework utilizing graph convolutional networks is utilized to achieve knowledge transfer from the simulation to the measured data, allowing for efficient fault detection of bearings with limited information. The main contributions of this study can be summarized as follows:

1) A dynamic simulation of the operational conditions of rolling bearings has been incorporated into a comprehensive and precise digital twin model.
2) A graph convolutional network-based transfer learning framework is developed to transfer knowledge from simulated dataset to measured data, so as to realize effective fault detection of bearings with limited knowledge.
3) Extensive experiments are conducted to validate the superiority of the developed DT-DAGN.

The rest of the article is organized as follows. Section II elaborates on the construction of the digital twin model. In Section III, a new transfer learning-based model called a domain adversarial graph network (DAGN) is presented in detail. Extensive experiments are conducted in Section IV to assess the performance of the developed approach. Finally, the conclusion and future research directions are discussed in Section V.

II. Digital Twin Model

A. Construction of Digital Twin Model

To accurately capture the dynamic response of the bearing system, a digital twin model has been developed. The model is a nonlinear dynamic representation of the rolling bearing, as shown in Fig. 2. It includes two degrees of freedom for

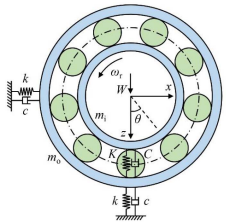

Fig. 2. Nonlinear dynamic model of rolling bearing.

both the inner and outer rings, namely horizontal translational displacement represented by x_i and x_o, and vertical translational displacement represented by z_i and z_o.

The rotating speed of the cage and the ball can be expressed as:

$$\omega_c = \frac{1}{2}\left(1 - \frac{d}{D}\cos\alpha\right)\omega_r \tag{1}$$

$$\omega_b = \frac{1}{2}\frac{D}{d}\left[1 - \left(\frac{d}{D}\cos\alpha\right)^2\right]\omega_r \tag{2}$$

in which the variables are defined as follows: the symbol d is used to represent the ball diameter, while D represents the diameter of the pitch. Additionally, α denotes the corresponding contact angle, and ω_r is used to indicate the rotor rotating speed.

The angular position of the jth ball can be obtained using the following equation:

$$\theta_j = \omega_c t + \frac{2\pi(j-1)}{N} \tag{3}$$

where the rolling ball's number is represented as N.

The contact deformation between the jth ball and raceways is given by:

$$\delta_j = (x_i - x_o)\sin\theta_j + (z_i - z_o)\cos\theta_j - \delta_c \tag{4}$$

where δ_c represents the initial radial clearance.

The horizontal and vertical Hertzian contact force between balls and raceways can be written as:

$$F_{sx} = \sum_{j=1}^{N} K\delta_j^{\frac{3}{2}}\sin\theta_j \cdot H(\delta_j) \tag{5}$$

$$F_{sz} = \sum_{j=1}^{N} K\delta_j^{\frac{3}{2}}\cos\theta_j \cdot H(\delta_j) \tag{6}$$

where K denotes the contact stiffness coefficient, and $H(\delta_j)$ indicates the Heaviside function and is expressed as:

$$H(\delta_j) = \begin{cases} 0, & \delta_j \le 0, \\ 1, & \delta_j > 0, \end{cases} \tag{7}$$

The horizontal and vertical contact damping force between balls and raceways can be written as:

$$F_{dx} = \sum_{j=1}^{N} C\dot{\delta}_j\sin\theta_j \cdot H(\delta_j) \tag{8}$$

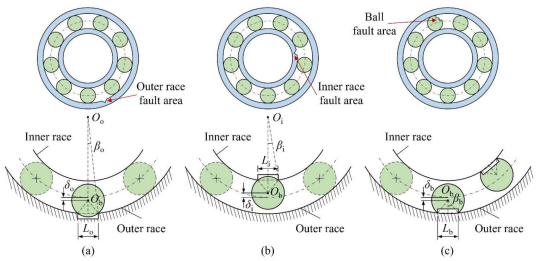

Fig. 3. Schematic of localized faults: (a) outer race defect, (b) inner race defect, (c) rolling ball defect.

$$F_{dz} = \sum_{j=1}^{N} C\dot{\delta}_j \cos\theta_j \cdot H\left(\delta_j\right) \tag{9}$$

where C represents the contact damping coefficient.

The following are the kinetic differential equations:

$$\begin{cases} m_i\ddot{x}_i + F_{dx} + F_{sx} = 0 \\ m_i\ddot{z}_i + F_{dz} + F_{sz} = W + m_i g \\ m_o\ddot{x}_o + c\dot{x}_o + kx_o - F_{dx} - F_{sx} = 0 \\ m_o\ddot{z}_o + c\dot{z}_o + kz_o - F_{dz} - F_{sz} = m_o g \end{cases} \tag{10}$$

where m_i and m_o are the mass of the inner ring and outer ring, respectively, k is the stiffness coefficient of the outer ring, c is the damping coefficient of the outer ring, and the variable W represents the radial load which is applied on the inner ring.

The dynamic model is designed to simulate three specific fault conditions, which are bearing outer ring fault, bearing inner ring fault, and bearing rolling ball fault. To simulate localized defects, circular spalls are used, as shown in Fig. 3.

Fig. 3(a) illustrates the outer race defect circumferential span angle, which can be formulated as:

$$\beta_o = arcsin\frac{L_o}{D_o} \tag{11}$$

the outer race defect width is denoted by L_o, and the diameter of the outer race is represented by D_o.

When the jth ball approaches the spall, their positional relationship can be described by the following expression:

$$mod\left(\theta_{OUT} - \theta_j, 2\pi\right) < \beta_o \tag{12}$$

here, θ_{OUT} represents the outer race defect angular position; $mod(\cdot)$ represents the modulus operator.

The deformation experienced by the ball as it passes the defect can be calculated using the following equation:

$$\delta_o = \frac{d}{2} - \sqrt{\left(\frac{d}{2}\right)^2 - \left(\frac{L_o}{2}\right)^2} \tag{13}$$

The following equation can be utilized to compute the relevant contact deformation that occurs between the ball and raceways as the ball passes over the defect of the outer race:

$$\delta_j = (x_i - x_o)\sin\theta_j + (z_i - z_o)\cos\theta_j - \delta_c - \delta_o \tag{14}$$

Fig. 3(b) illustrates the inner race defect circumferential span angle, which can be written as:

$$\beta_i = arcsin\frac{L_i}{D_i} \tag{15}$$

L_i is the inner race defect width, and D_i represents the inner race diameter.

When the spall is situated on the inner race, it rotates with the inner ring. The following equation expresses the positional relationship between the jth ball and the defect as the ball approaches:

$$mod\left(\theta_{IN} - \theta_j, 2\pi\right) < \beta_i \tag{16}$$

where θ_{IN} is the inner race defect angular position, and $\theta_{IN} = \omega_r \times t$.

As the ball passes over the inner race defect, it experiences a loss of contact deformation that can be quantified using the following calculation:

$$\delta_i = \frac{d}{2} - \sqrt{\left(\frac{d}{2}\right)^2 - \left(\frac{L_i}{2}\right)^2} \tag{17}$$

The following equation expresses the relevant contact deformation between the ball and raceways as the ball passes over the inner race defect:

$$\delta_j = (x_i - x_o)\sin\theta_j + (z_i - z_o)\cos\theta_j - \delta_c - \delta_i \tag{18}$$

The ball defect circumferential span angle can be seen in Fig. 3(c), and is given by:

$$\beta_b = arcsin\frac{L_b}{d} \tag{19}$$

where L_b is the ball defect width.

In the event that the spall is situated on the ball, it will travel along with the ball. As the ball defect approaches the outer race, the following expression can be used to describe the position relationship between the jth ball defect and the outer race:

$$mod\left(\phi_j - \frac{\pi}{2}, 2\pi\right) < \beta_b \tag{20}$$

The following equation provides the position relationship between the jth ball defect and the inner race as the ball defect approaches:

$$mod\left(\phi_j - \frac{3\pi}{2}, 2\pi\right) < \beta_b \tag{21}$$

where ϕ_j is the ball defect angular position, $\phi_j = \omega_b \times t$.

The contact deformation loss that occurs when the ball defect makes contact with either the outer race or inner race can be determined using the following calculation:

$$\delta_b = \frac{d}{2} - \sqrt{\left(\frac{d}{2}\right)^2 - \left(\frac{L_b}{2}\right)^2} \tag{22}$$

Using the previously calculated loss of contact deformation, one can derive the contact deformation that arises between the ball and raceways when the ball defect makes contact with either the outer race or inner race, as illustrated below:

$$\delta_j = (x_i - x_o)\sin\theta_j + (z_i - z_o)\cos\theta_j - \delta_c - \delta_b \tag{23}$$

TABLE I
STRUCTURAL PARAMETERS OF BEARING HRB 6205

Parameter	Value
Diameter of outer ring (D_o/mm)	46.98
Diameter of inner ring (D_i/mm)	31.10
Pitch diameter (D/mm)	39.04
Ball diameter (d/mm)	7.94
Number of rolling balls N	9
Contact angel (α/^{o})	0

TABLE II
KINEMATICS EQUATIONS THAT CORRESPOND TO BEARING FAULT FREQUENCIES

Fault condition	Characteristic frequency
Frequency of ball passing on the outer ring	$f_o = \frac{N}{2}(1 - \frac{d}{D}cos\alpha)f_r = 3.5848f_r$
Frequency of ball passing on the inner ring	$f_i = \frac{N}{2}(1 + \frac{d}{D}cos\alpha)f_r = 5.4152f_r$
Frequency of ball and pin interaction	$f_b = \frac{D}{d}[1 - (\frac{d}{D}cos\alpha)^2]f_r = 4.7135f_r$

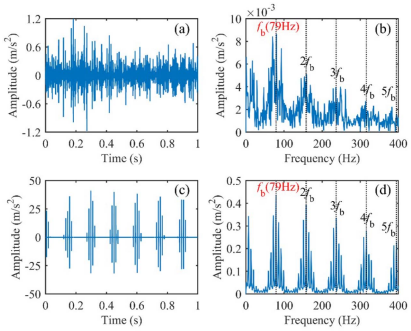

Fig. 4. Comparison of measured signal and simulated signal under rolling ball fault: (a) waveform of the measured signal, (b) envelope spectrum of the measured signal, (c) waveform of the simulated signal, (d) envelope spectrum of the simulated signal.

The vibration signal/response of the bearing system can be obtained by utilizing the fourth-order fixed-step Runge-Kutta algorithm to solve (10), with a calculation time step of 8.33 $\times 10^{-5}$ s.

B. Validation of the DT Model

Visual comparison of the simulated and measured vibration signals will confirm the validity of the digital twin model. This study aims to diagnose faults in the HRB 6205 rolling bearing using the vertical acceleration response. Table I presents the bearing's structural parameters, which are used to calculate the characteristic frequencies of the outer ring, inner ring, and rolling ball faults (Table II). Under a rotating speed of 1005 rpm, the measured and simulated signals for rolling element and inner ring faults are compared in the time-domain waveform and frequency-domain envelope spectrum, as presented in Figs. 4 and 5, respectively.

At a rotating speed of 1005 rpm, corresponding to a rotating frequency of $f_r = 16.75$ Hz, the theoretical fault frequencies

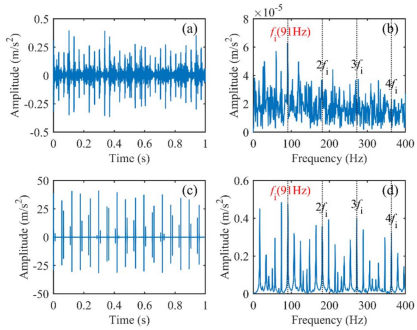

Fig. 5. Comparison of measured signal and simulated signal under inner ring fault: (a) waveform of the measured signal, (b) envelope spectrum of the measured signal, (c) waveform of the simulated signal, (d) envelope spectrum of the simulated signal.

for the rolling element and inner ring faults are 78.95 Hz and 90.70 Hz, respectively, based on the bearing parameters shown in Table I. The time-domain and frequency-domain envelope spectrum comparisons of the measured and simulated signals under the rolling element fault and inner ring fault are shown in Figs. 4 and 5, respectively. The time-domain vibration signals for both the measured and simulated signals exhibit periodic impulses when rolling bearing faults are present, as shown by the waveform graphs. Furthermore, the impulse characteristics of the measured and simulated vibration signals for each fault are quite similar. In the signal envelope spectrum, the fundamental frequencies of the simulated vibration signal match the theoretical values, and both the measured and simulated vibration signals exhibit the same frequency characteristics/components. These results indicate that the proposed digital twin model is highly effective in accurately reproducing the vibration response for various bearing fault types.

III. DOMAIN ADVERSARIAL GRAPH CONVOLUTIONAL NETWORK

A. Task Orientation

In the domain adaption task, labeled source domain dataset $D_s = X_s, Y_s = (x_i^s), (y_i^s)_{i=1}^{n_s}$ can be accessed, where n_s represents the number of samples and y_i^s corresponds the true label of x_i^s. Target domain dataset is represented by $D_t = X_t = (x_j^t)_{j=1}^{n_t}$, whose label cannot be accessed. Samples from two distinct yet interconnected probability distributions, designated as P and Q respectively, are used to gather data from both domains. Given that P and Q are distinct, the ultimate goal is to train a deep neural network, denoted as $h : X_t \rightarrow Y_t$, that can effectively generalize to the target domain. A domain adversarial graph network is developed for cross-domain fault detection of rolling bearings, as shown in Fig. 6.

B. Multiscale Graph Convolutional Network

This section presents the development of a multiscale graph convolutional network (MGCN) for feature extraction of mechanical signals, as illustrated in Fig. 7.

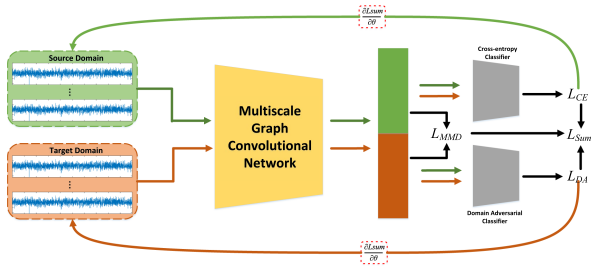

Fig. 6. Overall Architecture of the developed DAGN.

1) Multilevel Feature Extraction Block: The multilevel feature extraction block (MFEB) is constructed for multilevel learning of features, as shown in Fig. 8. Assuming K stands for MFEB's input, the initial step involves employing a 1×1 convolution for feature extraction, which can be expressed as follows:

$$K_1 = Conv_{1\times1}(K). \tag{24}$$

Afterwards, K_1 is evenly divided into four feature maps along the channel dimension, resulting in the following division:

$$K_2^1, K_2^2, K_2^3, K_2^4 = Split(K_1). \tag{25}$$

Subsequently, scale-correlated multi-scale learning is performed, which can be described as follows:

$$K_3^1 = Conv_{3\times1}^{r_1}\left(K_2^1\right), \tag{26}$$

$$K_3^i = Conv_{3\times1}^{r_i}\left(K_2^i + K_3^{i-1}\right), i \in \{2,3,4\} \tag{27}$$

where $Conv_{3\times1}^{r_i}(\cdot)$ denotes a $3\times$ 1 dilated convolution with the dilation rate r_i. Finally, the multi-scale features are combined by concatenating them and incorporating a residual connection, expressed as:

$$Y = Conv_{1\times1}\left(Concat\left(K_3^1, K_3^2, K_3^3, K_3^4\right)\right) + K, \tag{28}$$

Let Y denote the MFEB's output. All convolutions within MFEB are subsequently followed by batch normalization and ReLU activation.

2) Squeeze-and-Excitation Layer: Squeeze-and-excitation (SE) layer is adopted to guide the model to pay attention to important features. Let $I \in R^{C\times W}$ denote the input of the SE layer. Initially, the spatial details across all channels of the input are compressed into a single scalar through the following process:

$$q_s = \frac{1}{W}\left[\sum_{b=1}^{W} I_i(a,b)\right]_{a=1}^{C}, \tag{29}$$

Subsequently, a fully-connected block, consisting of two linear layers and two activation functions, is constructed to handle the accumulated information from the squeeze operation in the following manner:

$$q_e = Sigmoid\left(F_{mlp}(q_s)\right), \tag{30}$$

where $F_{mlp}(\cdot)$ stands for a two-layer connected layer. Finally, SE's output can be obtained via:

$$q_o = q_e \cdot I. \tag{31}$$

3) Overall Architecture of the MGCN: The overall architecture of the developed MGCN is displayed in Fig. 6. Given the input signal L. First of all, a 15×1 convolution is applied for the initial feature extraction of mechanical signals.

$$L_1 = Conv_{15\times1}(L), \tag{32}$$

where $Conv_{15\times1}(\cdot)$ stands for the 15×1 convolution, whose output channel number is 16. Then, several MFEBs combined with SE layers are utilized to extract more comprehensive local information.

$$L_2^1 = SE_1\left(MFEB_1(L_1)\right), \tag{33}$$

$$L_2^i = SE_i\left(MFEB_i\left(L_2^{i-1}\right)\right), i \in \{2,3,4\} \tag{34}$$

where $MFEB_i(\cdot)$ and $SE_i(\cdot)$ stand for MFEB operation and SE opearation, respectively. Further, multireceptive field convolutional layers are adopted to learn the structure information of the mechanical data.

$$L_3 = MRFConv\left(L_2^4\right), \tag{35}$$

$$L_4 = MRFConv\left(L_3\right), \tag{36}$$

where $MRFConv(\cdot)$ represents the multireceptive field convolutional operation. Finally, a classification layer is utilized for bearing health status classification.

C. Domain Adaption Classification Loss

1) Cross Entropy Loss: In order to guarantee a favourable prediction outcome for the label classifier, we estimate the classification loss by employing the cross-entropy loss. This loss serves as a measure of the dissimilarity between the true label and the predicted label, and it can be formally defined as follows:

$$L_{CE} = E_{\left(x_j^s, y_j^s\right)\sim D_s} L\left(C\left(x_j^s\right), y_j^s\right), \tag{37}$$

In the equation, $C(x_j^s)$ represents the predicted results of the label classifier.

2) MMD Loss: To align the feature structures of the source domain and target domain, we utilize the Maximum Mean Discrepancy (MMD) metric as a loss function for aligning their structural discrepancies. The MMD loss is denoted as follows:

$$L_{MMD} = \left|\left|E_{x_j^s\sim D_s}\left[\Phi\left(F\left(x_j^s\right)\right)\right] - E_{x_u^t\sim D_t}\left[\Phi\left(F\left(x_u^t\right)\right)\right]\right|\right|_{\Theta}^2 \tag{38}$$

where the symbol Φ stands for a nonlinear operation; and the distance is calculated by embedding the extracted features into the Reproducing Kernel Hilbert Space.

3) Domain Adversarial Loss: Due to the problem of domain covariate shift, the label classifier, when trained solely on data from the source domain, may not perform effectively on data from the target domain. To address this challenge, we introduce a domain discriminator (D) that determines whether the

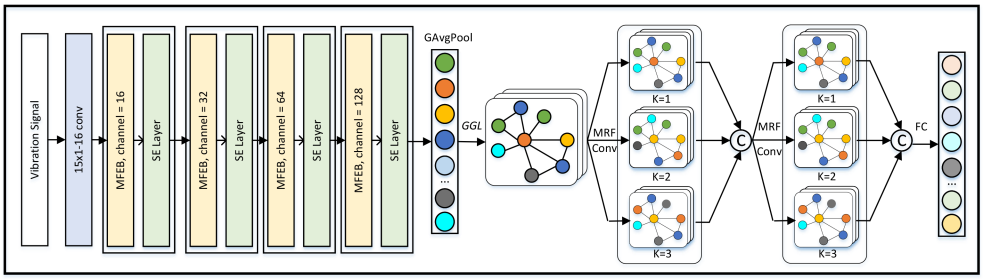

Fig. 7. Multiscale graph convolutional network.

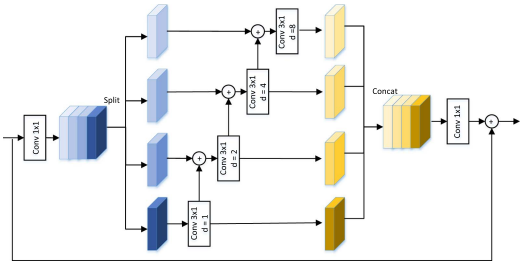

Fig. 8. Multilevel feature extraction block.

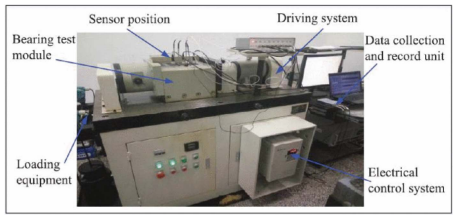

Fig. 9. ABLT-1 A bearing test bench.

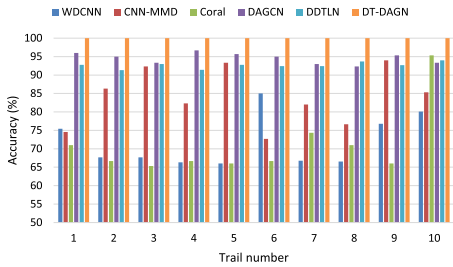

Fig. 10. Diagnostic accuracy of the six approaches in Task A.

extracted features originate from the source domain or the target domain. The feature extractor is trained to deceive the domain discriminator, enabling the capture of domain-invariant features as the two-player minimax game reaches equilibrium. In this context, the binary cross-entropy loss is employed as the domain alignment loss, which can be denoted as follows:

$$L_{DA} = E_{x_j^s} \sim D_s \left[log \left(1 - D \left(F \left(x_j^s \right) \right) \right) \right] + E_{x_u^t} \sim D_t \left[log \left(D \left(F \left(x_u^t \right) \right) \right) \right] \quad (39)$$

within the equation, $F(x_u^t)$ represents the extracted features of the u_{th} target sample, while $F(x_j^s))$ represents the extracted features of the j_{th} source sample.

4) Total Loss: By combining the three defined loss functions, the overall objective function can be expressed as follows:

$$L_{Sum} = L_{CE} + \chi L_{MMD} + \kappa L_{DA}, \quad (40)$$

in which χ and κ represent the tradeoff parameters.

IV. Experimental Verification

A. Experimental Settings and Data Description

The DT-DAGN code is implemented on a workstation with a GTX3060Ti GPU. During the training phase, we employ the Adam optimization algorithm with a learning rate of 0.005 and a batch size of 100. All experiments are carried out ten times to assure the fairness of the experiments. The DT-DAGN is compared with five competitive models:

1) *WDCNN:* WDCNN [32] is a popular CNN algorithm whose domain adaptation ability has been fully validated in the previous study.
2) *CNN-MMD:* CNN-MMD [25] is a classic domain adaption-based algorithm, which adopts maximum mean discrepancy (MMD) to realize effective fault detection.
3) *CNN-Coral:* CNN-Coral [33] utilizes a novel term namely the coral algorithm for cross-domain fault detection.
4) *DAGCN:* DAGCN [34] is a GCN-based domain adaption algorithm, which is effective for cross-domain fault diagnosis.
5) *DDTLN:* DDTLN [35] is a recently developed algorithm, which adopts a new joint distribution adaptation framework for machine fault identification.

In this study, the bearing dataset was collected from the ABLT-1 A bearing run-to-failure test bench, as depicted in Fig. 9. The bearing type used was HRB6205, and the motor speed was set to 1500 rpm. The dataset was sampled at a frequency of 12 kHz, and each sample contained 2048 data points. The dataset included three different states of rolling bearings: normal, ball fault, and inner ring fault, each comprising 800 samples. For training purposes, 300 samples were selected from each state, resulting in a total of 900 training samples. Similarly, for testing purposes, 100 samples were allocated to each state, resulting

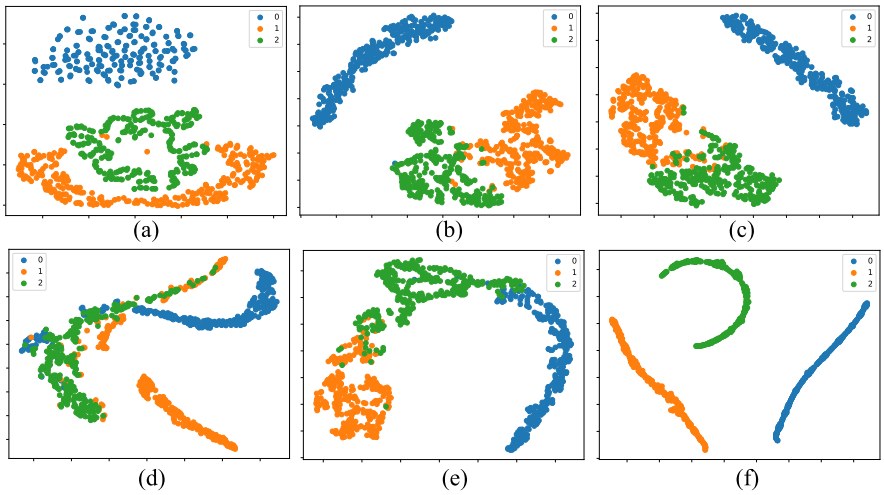

Fig. 11. Feature visualization via t-SNE: (a) WDCNN; (b) CNN-MMD; (c) CNN-Coral; (d) DAGCN; (e) DDTLN; (f) DT-DAGN.

TABLE III
DIAGNOSTIC ACCURACY OF THE SIX APPROACHES IN TWO TASKS

Approach	A → B [%]	B → A [%]
WDCNN	83.96 ± 7.76	68.03 ± 0.55
CNN-MMD	70.90 ± 9.08	68.50 ± 3.40
CNN-Coral	71.83 ± 6.93	60.14 ± 8.88
DAGCN	94.57 ± 1.46	81.33 ± 5.65
DDTLN	92.66 ± 0.84	76.80 ± 5.53
DT-DAGN	100.00 ± 0.00	91.20 ± 2.29

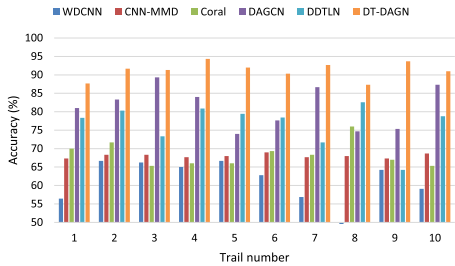

Fig. 12. Diagnostic accuracy of the six approaches in Task B.

in a total of 300 testing samples. The experiment involved two cases, namely Case A and Case B:

1) *Case A simulated data → measured data:* The simulated data at 1500 rpm was used as the source domain, and the measured data at 1500 rpm was used as the target domain.
2) *Case B measured data → simulated data:* The measured data at 1500 rpm was used as the source domain, and the simulated data at 1500 rpm was used as the target domain.

B. Experimental Results

The experimental results regarding Case A are displayed in Table III and Fig. 10. The DT-DAGN algorithm obtains 100% diagnostic results in all ten trials, which shows the stability of the DT-DAGN. Compared with WDCNN (83.96%), CNN-MMD (70.90%), CNN-Coral (71.83%), DAGCN (94.57%) and DDTLN (92.66%), DT-DAGN (100%) can obtain an overall accuracy gain of 16.04%, 29.1%, 28.17%, 5.43% and 7.34%, respectively, suggesting the superiority of the developed approach over the other five approaches. Further, we use feature visualization to gain a better understanding of the benefits of the proposed method. To achieve this goal, we employ t-SNE [36] technology to achieve the visualization of the features learned by the feature extractor. Fig. 11 displays the t-SNE results of the measured samples of all methods. Upon examining Fig. 11, it becomes clear that the features obtained by WDCNN are mixed together, resulting in many misclassification samples when the source model is used for the target domain test. Moreover, CNN-MMD, CNN-Coral, DAGCN and DDTLN exhibit overlapping features in different health conditions. On the contrary, the proposed method yields a feature distribution map that is more effective in discriminating between different classes and exhibits a distinct decision boundary.

The experimental results regarding Case B are displayed in Table III and Fig. 12. It is clear from Fig. 12 that the DT-DAGN algorithm respectively obtains 87.67%, 91.67%, 91.33%, 94.33%, 92%, 90.33%, 92.67%, 87.33%, 93.67% and 91% diagnostic results in all the ten trials. Regarding the overall average accuracy, compared with WDCNN (68.03%), CNN-MMD (68.50%), CNN-Coral (60.14%), DAGCN (81.33%) and DDTLN (76.80%), DT-DAGN (91.20%) can obtain an overall accuracy gain of 16.04%, 29.1%, 28.17%, 5.43% and 7.34%, respectively, suggesting the superiority of the developed approach over the other five approaches.

V. CONCLUSION

The detection and diagnosis of rolling bearing faults are crucial for the safe and efficient operation of rotating machinery, as they can result in significant economic losses and even accidents.

To address this issue, this article proposes a digital twin-based approach for intelligent rolling bearing fault diagnosis, utilizing a high-fidelity digital twin model to capture the dynamic response of the bearing under various health conditions. A transfer learning framework based on graph convolutional networks is then applied to transfer knowledge from simulated data to measured data, enabling effective fault detection of bearings with limited knowledge. Experimental results demonstrate the effectiveness of the proposed approach, which has the potential for broader industrial applications.

To address the complexity of failure mechanisms and the diversity of failure modes that can occur in real-world industrial scenarios, future research should aim to explore additional failure models and identify unknown fault modes within the corresponding target domain. Our future work will focus on refining the proposed digital twin model and validating the method with more bearing data.

References

[1] X. Li, Y. Xu, N. Li, B. Yang, and Y. Lei, "Remaining useful life prediction with partial sensor malfunctions using deep adversarial networks," *IEEE/CAA J. Automatica Sinica*, vol. 10, no. 1, pp. 121–134, Jan. 2023, doi: 10.1109/JAS.2022.105935.

[2] X. Yan and M. Jia, "Intelligent fault diagnosis of rotating machinery using improved multiscale dispersion entropy and MRMR feature selection," *Knowl.-Based Syst.*, vol. 163, pp. 450–471, 2019.

[3] Y. Xu and J. Hu, "Weak fault detection of rolling bearing using a DS-based adaptive spectrum reconstruction method," *J. Instrum.*, vol. 14, no. 03, 2019, Art. no. P03022.

[4] Y. Chen and M. J. Zuo, "A sparse multivariate time series model-based fault detection method for gearboxes under variable speed condition," *Mech. Syst. Signal Process.*, vol. 167, 2022, Art. no. 108539.

[5] W. Zhang and X. Li, "Data privacy preserving federated transfer learning in machinery fault diagnostics using prior distributions," *Struct. Health Monit.*, vol. 21, no. 4, pp. 1329–1344, 2022.

[6] Z. Chen et al., "A multi-source weighted deep transfer network for open-set fault diagnosis of rotary machinery," *IEEE Trans. Cybern.*, vol. 53, no. 3, pp. 1982–1993, Mar. 2023, doi: 10.1109/TCYB.2022.3195355.

[7] Y. Xu, X. Yan, B. Sun, J. Zhai, and Z. Liu, "Multireceptive field denoising residual convolutional networks for fault diagnosis," *IEEE Trans. Ind. Electron.*, vol. 69, no. 11, pp. 11686–11696, Nov. 2022, doi: 10.1109/TIE.2021.3125666.

[8] H. Wang, Z. Liu, D. Peng, M. Yang, and Y. Qin, "Feature-level attention-guided multitask CNN for fault diagnosis and working conditions identification of rolling bearing," *IEEE Trans. Neural Netw. Learn. Syst.*, vol. 33, no. 9, pp. 4757–4769, Sep. 2022.

[9] Y. Xu et al., "Cross-modal fusion convolutional neural networks with online soft label training strategy for mechanical fault diagnosis," *IEEE Trans. Ind. Inform.*, early access, Mar. 14, 2023, doi: 10.1109/TII.2023.3256400.

[10] Y. Xu, X. Yan, B. Sun, and Z. Liu, "Hierarchical multiscale dense networks for intelligent fault diagnosis of electromechanical systems," *IEEE Trans. Instrum. Meas.*, vol. 71, 2022, Art. no. 3505312, doi: 10.1109/TIM.2022.3150872.

[11] T. Han and Y.-F. Li, "Out-of-distribution detection-assisted trustworthy machinery fault diagnosis approach with uncertainty-aware deep ensembles," *Rel. Eng. Syst. Saf.*, vol. 226, 2022, Art. no. 108648.

[12] Y. Xu, X. Yan, B. Sun, and Z. Liu, "Dually attentive multiscale networks for health state recognition of rotating machinery," *Rel. Eng. Syst. Saf.*, vol. 225, 2022, Art. no. 108626, doi: 10.1016/j.ress.2022.108626.

[13] Y. Xu et al., "CFCNN: A novel convolutional fusion framework for collaborative fault identification of rotating machinery," *Inf. Fusion*, vol. 95, pp. 1–16, 2023, doi: 10.1016/j.inffus.2023.02.012.

[14] Y. Xu, X. Yan, B. Sun, and Z. Liu, "Deep coupled visual perceptual networks for motor fault diagnosis under nonstationary conditions," *IEEE/ASME Trans. Mechatron.*, vol. 27, no. 6, pp. 4840–4850, Dec. 2022.

[15] Y. Zhang, K. Feng, H. Ma, K. Yu, Z. Ren, and Z. Liu, "MMFNet: Multisensor data and multiscale feature fusion model for intelligent cross-domain machinery fault diagnosis," *IEEE Trans. Instrum. Meas.*, vol. 71, 2022, Art. no. 3526311.

[16] K. Zhao, J. Hu, H. Shao, and J. Hu, "Federated multi-source domain adversarial adaptation framework for machinery fault diagnosis with data privacy," *Rel. Eng. Syst. Saf.*, vol. 236, 2023, Art. no. 109246.

[17] Z. Chen, G. He, J. Li, Y. Liao, K. Gryllias, and W. Li, "Domain adversarial transfer network for cross-domain fault diagnosis of rotary machinery," *IEEE Trans. Instrum. Meas.*, vol. 69, no. 11, pp. 8702–8712, Nov. 2020, doi: 10.1109/TIM.2020.2995441.

[18] X. Li, W. Zhang, and Q. Ding, "Cross-domain fault diagnosis of rolling element bearings using deep generative neural networks," *IEEE Trans. Ind. Electron.*, vol. 66, no. 7, pp. 5525–5534, Jul. 2019, doi: 10.1109/TIE.2018.2868023.

[19] Y. Shi et al., "Transferable adaptive channel attention module for unsupervised cross-domain fault diagnosis," *Rel. Eng. Syst. Saf.*, vol. 226, 2022, Art. no. 108684.

[20] C. Yang, J. Liu, K. Zhou, M.-F. Ge, and X. Jiang, "Transferable graph features-driven cross-domain rotating machinery fault diagnosis," *Knowl.-Based Syst.*, vol. 250, 2022, Art. no. 109069.

[21] J. Chen, J. Wang, J. Zhu, T. H. Lee, and C. W. de Silva, "Unsupervised cross-domain fault diagnosis using feature representation alignment networks for rotating machinery," *IEEE/ASME Trans. Mechatron.*, vol. 26, no. 5, pp. 2770–2781, Oct. 2021.

[22] X. Li, W. Zhang, H. Ma, Z. Luo, and X. Li, "Deep learning-based adversarial multi-classifier optimization for cross-domain machinery fault diagnostics," *J. Manuf. Syst.*, vol. 55, pp. 334–347, 2020.

[23] X. Li, W. Zhang, H. Ma, Z. Luo, and X. Li, "Partial transfer learning in machinery cross-domain fault diagnostics using class-weighted adversarial networks," *Neural Netw.*, vol. 129, pp. 313–322, 2020.

[24] Y. Feng, J. Chen, S. He, T. Pan, and Z. Zhou, "Globally localized multisource domain adaptation for cross-domain fault diagnosis with category shift," *IEEE Trans. Neural Netw. Learn. Syst.*, vol. 34, no. 6, pp. 3082–3096, Jun. 2023.

[25] Y. Zhang et al., "Digital twin-driven partial domain adaptation network for intelligent fault diagnosis of rolling bearing," *Rel. Eng. Syst. Saf.*, vol. 234, 2023, Art. no. 109186.

[26] Y. Xiao, H. Shao, S. Han, Z. Huo, and J. Wan, "Novel joint transfer network for unsupervised bearing fault diagnosis from simulation domain to experimental domain," *IEEE/ASME Trans. Mechatron.*, vol. 27, no. 6, pp. 5254–5263, Dec. 2022.

[27] J. Wang, L. Ye, R. X. Gao, C. Li, and L. Zhang, "Digital twin for rotating machinery fault diagnosis in smart manufacturing," *Int. J. Prod. Res.*, vol. 57, no. 12, pp. 3920–3934, 2019.

[28] K. Feng, W. A. Smith, and Z. Peng, "Use of an improved vibration-based updating methodology for gear wear prediction," *Eng. Failure Anal.*, vol. 120, 2021, Art. no. 105066.

[29] K. Feng et al., "Vibration-based updating of wear prediction for spur gears," *Wear*, vol. 426, pp. 1410–1415, 2019.

[30] K. Feng, W. A. Smith, R. B. Randall, H. Wu, and Z. Peng, "Vibration-based monitoring and prediction of surface profile change and pitting density in a spur gear wear process," *Mech. Syst. Signal Process.*, vol. 165, 2022, Art. no. 108319.

[31] K. Feng, J. Ji, Y. Zhang, Q. Ni, Z. Liu, and M. Beer, "Digital twin-driven intelligent assessment of gear surface degradation," *Mech. Syst. Signal Process.*, vol. 186, 2023, Art. no. 109896.

[32] Z. Wei, G. Peng, C. Li, Y. Chen, and Z. Zhang, "A new deep learning model for fault diagnosis with good anti-noise and domain adaptation ability on raw vibration signals," *Sensors*, vol. 17, no. 3, 2017, Art. no. 425.

[33] Z. Huang et al., "A multi-source dense adaptation adversarial network for fault diagnosis of machinery," *IEEE Trans. Ind. Electron.*, vol. 69, no. 6, pp. 6298–6307, Jun. 2022, doi: 10.1109/TIE.2021.3086707.

[34] T. Li, Z. Zhao, C. Sun, R. Yan, and X. Chen, "Domain adversarial graph convolutional network for fault diagnosis under variable working conditions," *IEEE Trans. Instrum. Meas.*, vol. 70, 2021, Art. no. 3515010.

[35] Q. Qian, Y. Qin, J. Luo, Y. Wang, and F. Wu, "Deep discriminative transfer learning network for cross-machine fault diagnosis," *Mech. Syst. Signal Process.*, vol. 186, 2023, Art. no. 109884.

[36] L. Maaten and G. Hinton, "Visualizing data using t-SNE," *J. Mach. Learn. Res.*, vol. 9, no. 2605, pp. 2579–2605, 2008.

Ke Feng (Member, IEEE) received the Ph.D. degree from the University of New South Wales, Sydney, NSW, Australia, in 2021. He was with the University of British Columbia, Vancouver, BC, Canada, in 2022 and National University of Singapore, Singapore in 2023. His research interests include digital twins, vibration analysis, structural health monitoring, dynamics, tribology, signal processing, and machine learning. He is a Marie Curie Fellow of Imperial College London & Brunel University London. He is a Fellow of Vebleo. He is recognized as the Emerging Leader (2023) by Measurement Science and Technology journal. He is the Editor and Guest Editor of several journals, including *Mechanical Systems and Signal Processing*, IEEE TRANSACTIONS ON INDUSTRIAL CYBER-PHYSICAL SYSTEMS, *Engineering Applications of Artificial Intelligence*, IEEE TRANSACTIONS ON INSTRUMENTATION AND MEASUREMENT, *Measurement*, IEEE SENSORS JOURNAL, and *Measurement Science and Technology*.

Yadong Xu received the Ph.D. degree in mechanical engineering from Southeast University, Nanjing, China, in 2023. He is currently a Zijin Postdoctoral Researcher with the School of Mechanical Engineering, Nanjing University of Science and Technology, Nanjing. He has authored or coauthored more than 30 SCI-indexed papers such as *Information Fusion*, *Information Sciences*, IEEE TRANSACTIONS ON INDUSTRIAL ELECTRONICS, IEEE TRANSACTIONS ON INDUSTRIAL INFORMATICS, IEEE TRANSACTIONS ON MECHATRONICS, *Mechanical Systems and Signal Processing,* and *Reliability Engineering & System Safety*. His research interests include intelligent fault diagnosis, digital image processing, and pattern recognition.

Yulin Wang received the Ph.D. degree in mechatronics engineering from Shanghai Jiaotong University, Shanghai, China, in 2009. He is currently a Professor with the School of Mechanical Engineering, Nanjing University of Science and Technology, Nanjing, China. His research focuses on intelligent manufacturing.

Sheng Li is currently working toward the Ph.D. degree in industrial engineering from Hohai University, Nanjing, China. He is also a visiting Ph.D. student with the University of British Columbia, Vancouver, BC, Canada. His research interests include intelligent fault diagnosis, digital image processing, and pattern recognition.

Qiubo Jiang received the B.S. degree in vehicle engineering from Southwest University, Chongqing, China, in 2016 and the M.S. degree in vehicle engineering from China Agricultural University, Beijing, China, in 2020. He is currently working toward the the Ph.D. degree in mechanical engineering from Southeast University, Nanjing, China. His research interests include digital twins, fault diagnosis, and nonlinear dynamics.

Beibei Sun received the Ph.D. degree in mechanical engineering from Southeast University, Nanjing, China, in 2001. She is currently a full Professor and Doctoral Supervisor with the School of Mechanical Engineering, Southeast University. Her research interests include digital image processing, machine learning, dynamics of complex electromechanical systems, and dynamic optimization design of construction machinery.

Jinde Zheng received the Ph.D. degree in mechanical engineering from Hunan University, Changsha, China, in 2014. He is currently a Professor with the Anhui University of Technology, Maanshan, China. His research interests include machinery health monitoring and fault diagnosis, statistical signal processing, and complexity theory.

Qing Ni received the Ph.D. degree from the School of Mechanical and Mechatronic Engineering, University of Technology Sydney, Ultimo, NSW, Australia, in 2022 and the M.S. degree from the School of Mechanical and Electrical Engineering, University of Electronic Science and Technology of China, Chengdu, China, in 2019. She is currently a Postdoctoral Research Associate with the University of Technology Sydney, Ultimo, NSW, Australia. Her research interests include equipment reliability & health management, signal processing, machine learning, fault diagnosis, remaining useful life prediction, and digital twin. She is the Guest Editor of several journals, such as *Engineering Applications of Artificial Intelligence*, *Computer Systems Science and Engineering*, and *Measurement Science and Technology*.